Nuclear Inst. and Methods in Physics Research B 462 (2020) 24–31

Contents lists available at ScienceDirect

Nuclear Inst. and Methods in Physics Research B

journal homepage: www.elsevier.com/locate/nimb

Neutron radiobiology studies with a pure cold neutron beam

M. Pedrosa-Rivera[a,b,*], M.J. Ruiz-Magaña[c], I. Porras[b], J. Praena[b], P. Torres-Sánchez[b], M.P. Sabariego[b], U. Köster[a], T. Forsyth[a], T. Soldner[a], M. Haertlein[a], C. Ruiz-Ruiz[c]

[a] Institut Laue-Langevin, Avenue des Martyrs, 38042 Grenoble, France
[b] Departamento de Física Atómica Molecular y Nuclear, Facultad de Ciencias, Universidad de Granada, 18071 Granada, Spain
[c] Departamento de Bioquímica y Biología Molecular III e Inmunología, Facultad de Medicina, Universidad de Granada, 18071 Granada, Spain

ARTICLE INFO

Keywords:
Neutron radiobiology
BNCT
Cold neutron beam
A375 melanoma cells

ABSTRACT

Data on the radiobiological effects of thermal neutrons are usually obtained from irradiations in a mixed field of neutrons of different energies and gamma rays or from conversion of proton data with similar energies to those created in the neutron capture on nitrogen. Experimental data from irradiations in a pure thermal or cold neutron beam can help to find new values for neutron relative biological effectiveness (RBE) factors, which are useful for BNCT (Boron Neutron Capture Therapy) and radiation protection applications. We present a new experimental setup for radiobiological studies at a cold neutron beam at Institut Laue-Langevin, a beam without fast neutron component and almost no gamma ray contribution. After the irradiation, survival assays are performed to obtain the survival curves. Finally, comparing with a reference photon irradiation, the thermal neutron RBE factors can be calculated. The methodology is outlined at the example of A375 melanoma cells for which new radiobiological data were obtained.

1. Introduction

The estimation of the biological damage produced by neutrons is not an easy problem to solve. As neutrons ionize indirectly, the key point for the biological study is the effect of the secondary particles after the collisions and nuclear reactions produced by them in the tissue, which depend on the neutron energy. The knowledge of biological damage of neutrons is useful for radioprotection, but also a key factor for therapies with neutrons like Boron Neutron Capture Therapy (BNCT).

BNCT is an experimental form of selective radiotherapy which is currently regaining interest because of the most recent promising clinical trials [1], and the development of new in-hospital accelerator-based neutron sources that may bring this therapy closer to the clinical practice [2].

Treatment planning in BNCT is based on figures of the so-called weighted (or photon equivalent) dose. This is obtained by weighting the different absorbed dose components by means of relative biological effectiveness (RBE) weighting factors, usually denoted by w_i, such that the weighted dose D_W is given by

$$D_W = w_f D_f + w_t D_t + w_\gamma D_\gamma + w_B D_B \quad (1)$$

The dose components are [3,4]: the fast dose, D_f, from the secondary particles produced by neutrons with energy above 0.5 eV, i.e. mainly hydrogen recoils; the thermal dose, D_t, by neutrons with energy below 0.5 eV, mainly due to neutron capture on nitrogen, but excluding capture on boron ; the boron dose, D_B, due to the products of the boron capture reaction, mostly from thermal neutrons, and the gamma dose, D_γ, which includes photons both from contamination of the beam and from radiative captures produced in the tissue. The weighting factors, w_i, are obtained from a comparison between the dose given by the neutrons and a reference photon dose, for a specific survival. No synergies between the different components are included.

The weighting factors currently used have been those proposed by Coderre and Morris [5], based on radiobiology experiments focused on the application to brain tumors [6]. Thus, the weighting factor for the dose components in tumors are taken from the values obtained for clonogenic assays of the rat 9L gliosarcoma. These values have also been applied in other clinical BNCT trials, for instance with head and neck cancers and melanoma, pending direct validation by means of new experimentation with different tissues and/or cell types.

Moreover, in the experiments mentioned above, the irradiations were performed with a mixed beam containing both fast and thermal neutrons, which means that their effects could not be distinguished [7]. The neutron spectra of some of these beams are shown in Fig. 1. It has been argued that the thermal and fast neutron weighting factors are

* Corresponding author at: Institut Laue-Langevin, Avenue des Martyrs, 38042 Grenoble, France.
E-mail address: mpedrosa@ugr.es (M. Pedrosa-Rivera).

https://doi.org/10.1016/j.nimb.2019.10.027
Received 5 September 2019; Received in revised form 17 October 2019; Accepted 23 October 2019
Available online 08 November 2019
0168-583X/

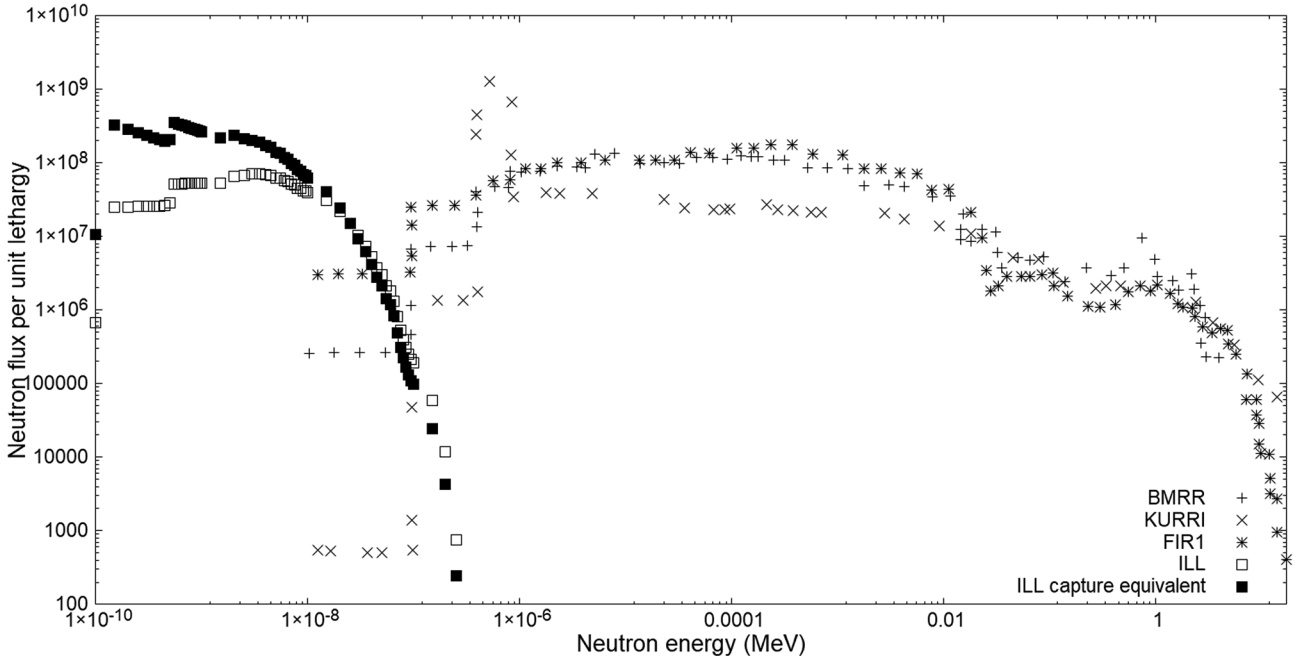

Fig. 1. Neutron spectra of some BNCT beams [13] in comparison with the ILL Pf1b cold neutron beam. ILL data corresponds to the beam in June 2018 with a total capture equivalent flux of $1.75 \cdot 10^9 n_{th}/cm^2 s$ measured.

similar due to comparable energy of the recoil proton from the elastic collisions of the fast neutrons and the energy of the protons released from the thermal neutron capture on nitrogen (584 keV) [5]. For this reason, w_f and w_t have been considered equal in all the clinical trials performed so far. However, more recent studies with protons of similar energies as those coming from the two processes suggest that this assumption should be reviewed [8].

The weighting factor, w_t (as well as the boron dose weighting factor, w_B), is a factor independent of the neutron beam spectrum. Its accurate determination is very important as it can be used at any BNCT facility, whilst the fast neutron factor could depend on the particular beam spectrum. Radiobiology studies with epithermal beams have shown a strong energy-dependence [9,10], therefore the fast neutron RBE should be measured at each BNCT facility. But even for the measurement of w_f itself from an epithermal neutron beam, prior knowledge of the w_t factor is required for correcting the effect of the neutrons that thermalize in the sample.

Thermal neutron data can be obtained at reactors providing thermal neutron beams from tangential beam tubes facing the water moderator (either in the pool or tank) or so-called thermal columns. These are beam tube inserts from e.g. graphite, that provide a well-thermalized neutron spectrum, like at the BMRR reactor in Brookhaven [11] or LENA in Italy [12]. However, even such beams are accompanied by a non-negligible gamma component due to neutron captures in the moderator as well as Compton scattered energetic gamma rays from the reactor core. Differential measurements of the radiobiological effect of neutrons alone are therefore challenging and intrinsically affected by larger uncertainties from the background deduction, which cannot be linearly subtracted as the photon biological effect is known to be described by a linear-quadratic model.

Few high flux reactors and spallation neutron sources are equipped with so-called neutron guides where neutrons are efficiently transported over large distances by total reflection on a vacuum-matter interface. These neutron guides are slightly bent to prevent a direct view on the source. Only thermal and slower neutrons can follow the curvature by total reflection while faster neutrons and gamma rays go straight and are stopped in the shielding of the neutron guide. Thus, at the exit of such guides the initial component of epithermal and fast neutrons as well as gamma rays from the reactor are completely suppressed. Some background is still produced locally by interactions of the neutron beam, but when taking care in the selection of beam windows (separating the vacuum of the neutron guide from the experimental setup), beam stop (downstream of the setup) and surrounding material, the total background from gamma rays and fast neutrons can be minimized. Certain reactors are equipped with a so-called cold source where a vessel containing e.g. liquid deuterium (25 K) is introduced on purpose to moderate neutrons to a lower energy. Beam tubes facing such a cold source will extract cold neutrons, corresponding to average neutron energies of few meV, i.e. lower than thermal energies. Due to larger critical angles cold neutrons can be more efficiently guided than thermal neutrons and higher beam intensities are available for experiments.

One such beam, called PF1b, exists at Institut Laue-Langevin (ILL) in Grenoble. Experiments that study nuclear reactions induced by neutron capture or the effects thereof are performed there. For nearly all neutron capture reactions the cross-section follows at low energies (thermal and below) a perfect 1/v behavior, where v is the neutron velocity. Therefore, cold neutrons can fully replace thermal neutrons as long as the so-called thermal-equivalent capture flux (or just capture flux) is used, expressed in $n_{th}/cm^2 s$ (see Fig. 1). For comparison with other experiments using “true” thermal neutron beams we will use in the following the term “thermal neutron effects” for our results, although technically speaking they have been obtained at a cold neutron beam.

In this work, we show a procedure for using the PF1b line at ILL for the irradiation of cells with a very pure thermal-equivalent neutron beam. Without fast neutrons or gamma rays coming from the beam, this line will allow the determination of the RBE factor with less uncertainly, as the only non-desired gamma contribution comes from the (unavoidable) photons produced in the sample, which will be minimized in our set-up.

A demonstration of the ability to perform accurate measurement of the w_t factor will be shown in a test case, the A375 human melanoma cell line. This is a relevant test case because it corresponds to a cell line sufficiently different from rat gliosarcoma from which the accepted values were taken [6], while it is still representative of an actual application of BNCT.

2. Materials and methods

2.1. The cold neutron line PF1b

The reactor at Institut Laue-Langevin is equipped with so-called neutron guides where neutrons are efficiently transported over large distances by total reflection on a vacuum-matter interface. As mentioned above, the PF1b cold neutron line [14] has been chosen for the irradiation of cells because the absence of contamination from both gammas and fast neutrons due to its bent guide.

The capture flux is determined by an activation experiment, of e.g. a thin gold foil (12–14 μm). As this reaction follows a 1/v behavior one uses the thermal ^{197}Au(n,γ)^{198}Au cross-section of 98.7b to derive from the measured ^{198}Au activity the capture flux. Irrespective of the exact neutron spectrum the number of neutron captures in thin samples will always correspond to that in a pure thermal neutron beam of the same capture flux. For a cold neutron beam of 4 meV average energy the average neutron velocity is 880 m/s, i.e. a factor 2.5 smaller compared to a thermal neutron beam with 25 meV average energy and average neutron velocity of 2200 m/s.

While the number of captures in a thin sample is perfectly described by the capture flux, it is evident that there will be less neutrons passing per cm^2 per second than for a true thermal beam. The actual particle flux is smaller by the very same factor 2.5 as the cross-section is larger than the thermal cross-section. If very thick samples are used, cold neutron beams experience a stronger attenuation than thermal neutrons and they also change their spectrum ("beam hardening") due to more pronounced attenuation of slower neutrons and partial up-moderation to the temperature of the sample. Ultimately, for infinitely thick samples, the particle flux determines the total number of captures per second and not the capture flux.

The experiments described in the following represent an intermediate of both cases: the cell layer represents a thin sample where the number of captures and, thus, the radiobiological effects of the neutrons, are very well described by the capture flux. When a stack of multiple vials with individual cell layers is used, the actual neutron spectrum has to be considered to determine the attenuation of the neutron flux from one vial to the next while for the number of captures in every cell layer again the local capture flux is used. The attenuation calculation has been performed by Monte Carlo simulations with the MCNPX code and validated by gold foil activations placed at the respective positions of cell layers.

The initial beam leaving the PF1b neutron guide was collimated by a 3 m long set of ^{10}B and ^{6}Li containing diaphragms to obtain a pencil-like beam of 2 cm diameter (Fig. 2). All boron diaphragms were doubled with 5 cm thick lead diaphragms to avoid gamma contamination of the beam. All diaphragms close to the sample and the beam stop were made from ^{6}LiF to prevent gamma background. Without samples present, the capture flux at the sample position, measured by gold foil activation, was 1.8x10^9 n_{th}/cm^{2}s. Therefore, with the bent guide and

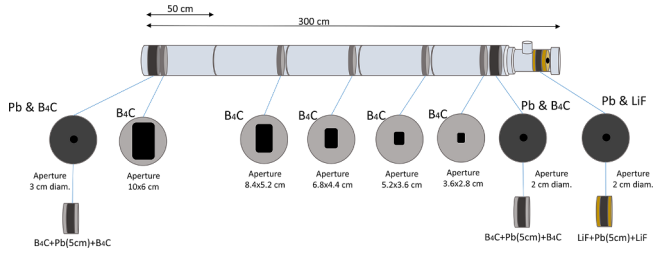

Fig. 2. Collimation system situated at the end of the bent guide. The neutron beam at the end of the collimation is 2 cm in diameter. Secondary gammas created by captures on boron collimators are stopped in the lead layers. The last collimator is made from LiF to capture neutrons without secondary gamma emission.

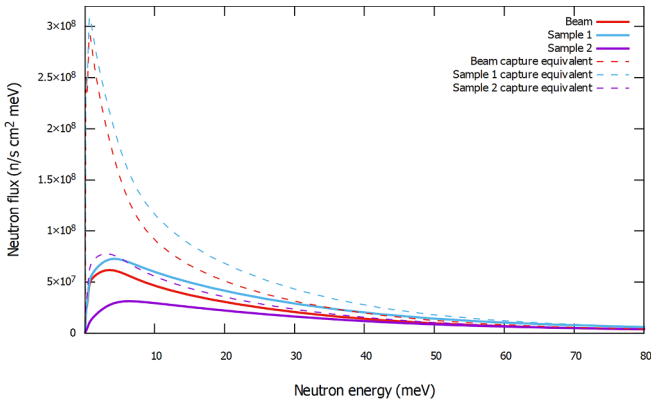

Fig. 3. PF1b beam spectrum (red) and the spectrum in the two samples irradiated simultaneously (sample 1 in blue and sample 2 in purple), per meV. Dashed lines correspond to the capture equivalent spectrum (per meV) of the beam and each sample. Data corresponds to the beam in June 2018, with a total capture equivalent flux of $1.75 \cdot 10^9 n_{th}/cm^2 s$ measured. (For interpretation of the references to colour in this figure legend, the reader is referred to the web version of this article.)

the collimation system, that results in a gamma background of less than 2% of the beam, the gamma component will be due to the set-up components situated after the collimation (samples and sample holders)

The beam alignment and homogeneity was checked by radiochromic films (Gafchromic EBT2). Films were irradiated at different irradiation times to calibrate the grey level as function of capture fluence. Subsequently, the grey levels across the beam spot were analyzed to check the homogeneity of the beam. Deviations from the average flux are on average less than 2%, see Fig. 4. A detailed description of a very similar collimation system used for prompt gamma ray spectroscopy at the PF1b beam line can be found in [15]. The present collimation system used wider diaphragms (20 mm diameter instead of 12 mm) over a shorter distance (2.5 m instead of 5 m) leading to a significantly higher capture flux at the target position.

In Fig. 3 both the simulated particle flux and capture flux at the exit of the collimator system at PF1b line are displayed.

2.2. Irradiation Set-up

Cells are placed in 100-QS 2 mm Hellma Suprasil absorbance quartz cuvettes. This hydrogen-free vessel minimizes neutron scattering while the neutron capture cross-sections in silicon and oxygen are small enough to minimize production of gamma rays in the material. The cuvettes have a 2 mm empty space which is used to place the cells with minimal amount of culture medium (200 μl). To assure a thin cell layer on a well-defined side of the cuvette, the cuvette is placed horizontally for 24 h after filling. The low thickness of the cuvette allows keeping the medium at the bottom, even when the cuvette is placed horizontally. Any adherent cell type will thus attach just to the bottom side.

For the irradiation, the quartz cuvettes are filled with fresh media and placed upright in a Teflon holder with the side of the adhering cell layer facing the beam (see Fig. 3). Two samples are irradiated at the same time, where the downstream one receives about half of the dose compared to the first one. This allows obtaining two survival points per irradiation time. Although the relative gamma dose component (in our experiments mainly due to the capture on hydrogen in the medium and in the cells) increases from the first to the second cuvette, it is still smaller than the neutron dose component (see Table 2). The scheme of the setup is illustrated in Fig. 5.

The doses received by both cell layers are estimated by means of a Monte Carlo simulation performed with the MCNPX code [16] using the neutron beam spectrum, the set-up geometry and the corresponding materials. The neutron spectrum after the collimation system was

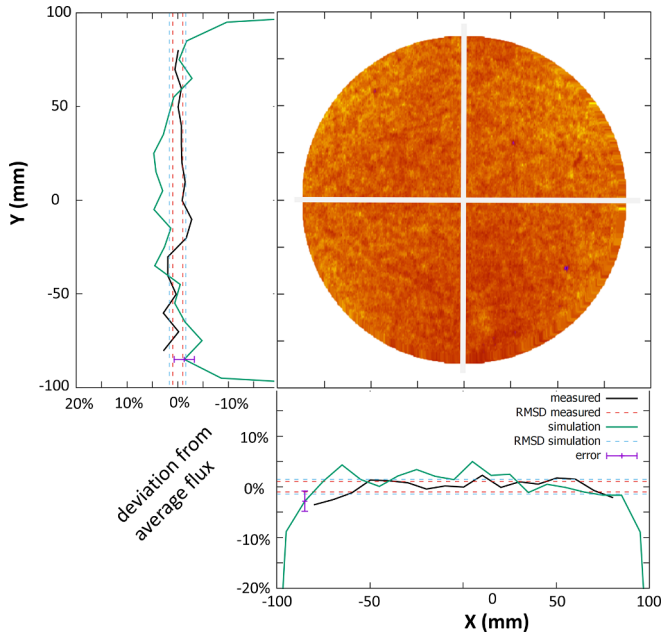

Fig. 4. Measured beam at sample1 position. The 3D profile is extracted from the radiochromic films scanned. The figure and data correspond to the measured results of a film irradiated for 80 s, compared to the simulated data in the graphs. The deviation from the average flux along the x and y axis is represented, with an error on the simulation of ± 0.02, shown with error-bars in one of the points. Root-mean-square deviation (RMSD) is indicated (in both cases, measured and simulation, it is less than 3%).

calculated with the McStas neutron transport software [17]. For dose estimation, neutron kerma factors are calculated for ICRU-33 tissue with H, C, N, O based on cross sections from ENDF/B-VII and photon kerma factors from Seltzer X-ray [18] mass attenuation data. Final dose components were calculated from the fluence provided by the MCNPX simulation convoluted with the calculated neutron kerma factors [4]. Secondary fast neutrons created in nuclear reactions induced by the charged particles produced by neutron captures in both Li and B respectively [19] of the shielding are shown to contribute far less than 1% to the dose (See Table 1). The effect of a non-perfect Charged Particle Equilibrium (CPE) achieved, where about 20% of the dose from protons after neutron captures in the cells is deposited outside the cell layer, is included (for a cell layer of 15 μm thickness, the calculated effect amounts to 18.5%). The doses are calculated for a nitrogen composition of 4.6% (mass fraction) for skin cells [20].

In the simulations, photons from neutron capture are also transported and the gamma dose produced at the cells has been calculated,

Table 1
Undesired dose component analysis to design the final set-up. First, gamma dose at the sample 1 due to neutron capture in the different materials, and second, fast dose on the sample 2 (nearest to beam stopper) due to neutron captures in LiF of the beam stopper [19]. When there is only the beam and a layer of cells, the gamma dose component is less than 1% of the total dose (Table 2). By adding the culture media (necessary for the cells to survive), for 2 mm of media, the gamma dose jumps to 12% of the total dose. The quartz cuvette to contain the cells and the media increases the gamma dose component to 19%. Finally, by adding the second quartz, to leverage beam time by irradiating two samples at same time, the gamma dose goes to 21% of the total dose. The fast dose from neutron captures in Li in the beam stopper is negligible when the beam stopper is at the real position, and remains negligible even when the beam stopper is placed just after the sample 2. Uncertainties of the dose calculations are explained in the caption of Table 2.

Set-up	Gamma dose (Gy/h) in cuvette 1
Beam + cells	0.026
Beam + cells + 2 mm culture media	0.446
Beam + cells + 2 mm culture media + quartz cuvette	0.702
Beam + 2 complete quartz cuvettes (real Set-up)	0.784
Set-up	**Fast Dose (Gy/h) in cuvette 2**
Beam stopper at 8.1 cm (real Set-up)	10^{-6}
Beam stopper at 0.01 cm	10^{-4}

as well as the pure neutron dose. The gamma dose, produced mainly from captures on hydrogen in the culture medium and cells, is estimated to be around 21% of the total physical dose for the first sample and 30% for the second (values displayed in Table 2). This means a great improvement with respect to previous in vitro measurements performed at other facilities, e.g. at the thermal column of BMRR, from where the reference values used in BNCT were obtained, where the gamma component was greater than the thermal (called nitrogen) dose component [5].

In addition to the neutron flux measurements with gold foils, the relative doses obtained in the simulations were confirmed when results of cuvette 1 irradiated for 40 min (simulated dose of 2.51 Gy) were compared with those from cuvette 2 irradiated for 75 min (simulated dose of 2.46 Gy). In Fig. 7, similar survival and proliferation data can be seen for both cases.

The dose rate obtained allows performing cell survival experiments for reasonable irradiation times. The effect of the gamma component will be subtracted accordingly with the linear-quadratic model in order to extract the pure neutron effect.

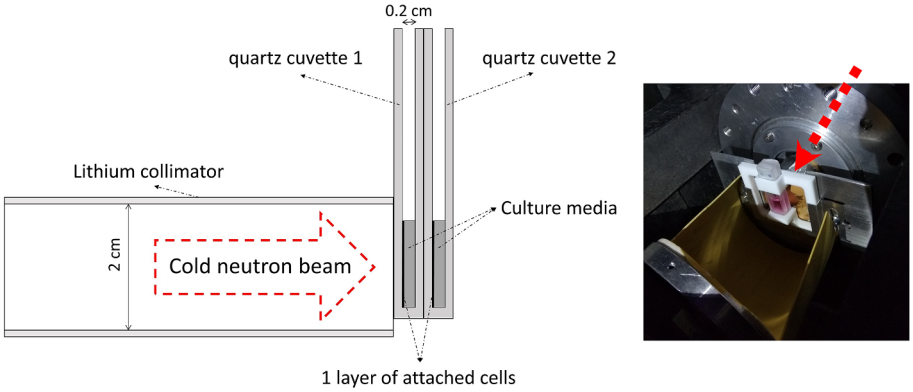

Fig. 5. Schematic cut view of the setup used in the experiments and simulations (left drawing) and a picture (right) of the irradiation holder placed at the exit of the beam line with the cuvettes filled with cells and culture medium.

Table 2
Dose rate delivered at the melanoma cells during the irradiations at the two positions. The statistical uncertainties from the fluence from Monte Carlo simulations are less than 1% and the error of the kerma factor used to calculate the dose is less than 5% (ICRU recommendations). The good temporal stability of the beam and the stable positioning of the samples add a systematic error of no more than 3%. The neutron shutter was operated manually which introduces a scatter in effective irradiation time of 2% on average (up to 5% for the shortest irradiations). An assumed thickness variation of ± 10% of the cell layer (13.5 to 16.5 μm) results in ± 2% uncertainty of the incomplete CPE correction of the thermal dose. The actual irradiation times are logged with 1 s resolution, but due to the nonlinear dose-effect relationship we refrained from rescaling the results of slightly different irradiation times and rather consider this scatter as a statistical uncertainty in dose. This data corresponds to the flux in June 2018. Data must be adapted depending on the actual capture flux during the irradiation cycle, which is determined with gold foil measurements.

Sample	Thermal neutron dose rate (Gy/h)	Gamma dose rate (Gy/h)	Fast neutron dose rate (Gy/h)	Total dose rate (Gy/h)
Cells in cuvette 1	2.942	0.784	10^{-6}	3.726
Cells in cuvette 2	1.374	0.588	10^{-6}	1.962

2.3. Cell culture and survival studies

A level 2 biological lab has been installed in the same instrument hall as the PF1b beam line to facilitate the sample management. The new lab and beam line are within 1 min walking distance, thus enabling high sample throughput per day.

For the neutron irradiations, $2x10^5$ cells in 200 μl complete medium are placed inside 2 mm thick quartz cuvettes. After 24 h, cells are naturally attached in one layer inside the quartz cuvettes. Before the irradiation, the culture medium is replaced.

After the irradiation, clonogenic assays are performed. Cells are detached with 1% trypsin-EDTA (Sigma-Aldrich, St Louis, MO, USA) and suspended in complete culture medium. Cells are then seeded into 6-well plates at different densities, as the plating efficiency varies with the cell line and the irradiation. In the example case of A375 cells, after 7–8 days, colonies were fixed with 90% ethanol at room temperature and stained with crystal violet (1% w/v) for 30 min. Crystal violet was removed carefully, the plates were immersed in tap water to rinse off the dye. Colonies containing more than 50 cells are counted and surviving fractions are calculated. All assays are performed in triplicates.

Finally, in order to obtain results for a second biological end-point, a cell proliferation assay can be also performed after irradiation by means of the BrdU Cell Proliferation ELISA kit (Roche, Mannheim, Germany). Briefly, A375 cells (1×10^3/well) were seeded into 96-well plates and grown for 96 h and proliferating cells were determined according to the manufacturer's protocol.

The A375 cell line was kindly provided by Dr. Lucie Sancey (Institute for Advanced Biosciences, Grenoble). Cells were cultured in RPMI medium (HyClone, Logan, USA) containing 10% fetal bovine serum (FBS; Gibco, California, USA), 1 μM L-glutamine (Gibco, California, USA) and 100 IU/ml penicillin and 100 IU/ml streptomycin (Sigma-Aldrich, St. Louis, USA) at 37 °C in a humidified 5% CO_2, 95% air incubator.

3. Example of application: A375 cell line

3.1. Survival after neutron irradiation by clonogenic assay

A set of irradiations from 15 to 82 min were carried out which resulted in doses in the range of 0.48–5.1 Gy. After each irradiation, a clonogenic assay was performed. An example of the colony growth in response to two different irradiation doses is shown in Fig. 6.

The survival was expressed according to the plating efficiency of the control sample for each irradiation. Results in Fig. 7 show that, even at low doses of less than 1 Gy, there was a strong effect with around 50% of cells surviving. At a neutron fluence of 3.7×10^{12} n/cm^2, which corresponds to a dose of around 2.8 Gy, the survival fraction was 10%. These results are an illustration of the strong effect of the low energy neutron irradiation compared with that of the photon one where, in most of cell lines, more than 4 Gy are required to reach a 10% of survival.

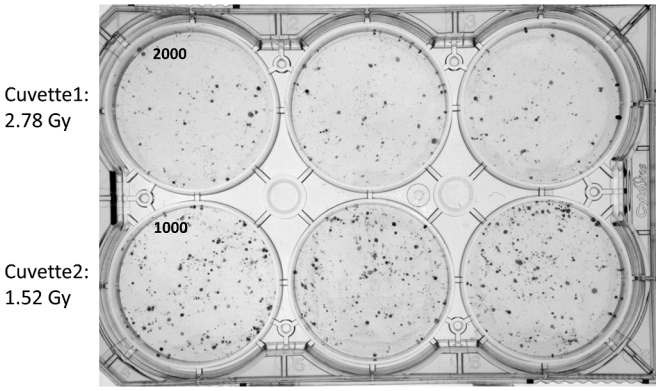

Fig. 6. Colonies formed by A375 cells at 7 days after the irradiation. The bottom row of samples received a lower dose than the top row. The increase in the number of colonies, i.e. higher survival, is clearly observed, even though the amount of cells seeded (number on the top of the first well) is less for the low doses.

3.2. Cell proliferation after neutron irradiation

As a second biological end-point, we performed a BrdU assay which shows all the cells that are viable and can proliferate. Proliferating A375 cells at 96 h after neutron irradiation are shown in Fig. 7. There was a strong decay in the amount of proliferative cells after 3 Gy irradiation. A 70% inhibition of cell proliferation was observed at the highest dose.

A375 cells are known to be very resistant to X-ray radiation. For example, in a recent study, 60% of viable cells were still found after delivering 2 Gy of X-ray radiation, and nearly 40% of cells were viable in response to 6 Gy [21]. From our data, it seems that neutron irradiation is more effective in reducing cell proliferation as, with doses of around 4 Gy, the fraction of viable cells drops to less than 30%.

3.3. Determination of the thermal neutron RBE weighting factor

As the colony formation ability is the common biological endpoint chosen for survival studies in radiobiology, the results from the clonogenic assay have been chosen for deriving the RBE factor.

For the analysis, several assumptions are made: First, the photon spectrum produced by the neutron beam has the same radiobiological effectiveness as the photon spectrum used in gamma-ray irradiations, for which results exist in the literature. Therefore, the parameters used for the reference photon dose will be the same as those used for the gamma component of the beam. Second, following the current formalism shown in Eq. (1), no synergies are involved, ergo the effects on the cells are independent between different secondary particles. Third, survival curves are fitted following the linear-quadratic model [22], with the quadratic component neglected for the high LET component (pure neutron).

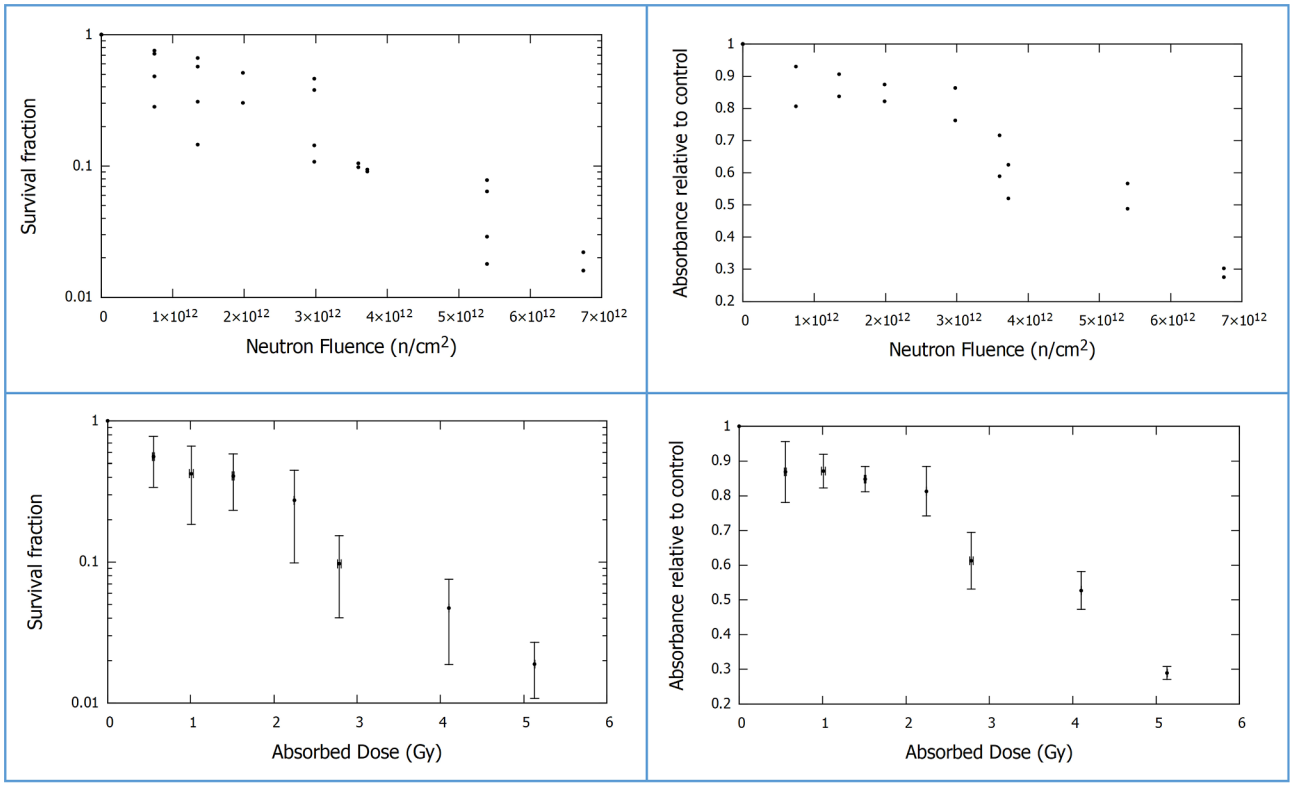

Fig. 7. Left: Survival fraction of the different samples of A375 cells after different irradiation times as a function of the neutron fluence. Then, survival data corresponding to similar doses are grouped and represented as a function of the total absorbed dose, which includes the gamma dose component. Cells attached in one layer inside quartz cuvettes were homogeneously irradiated and the surviving fraction was determined by clonogenic assay. Right: BrdU proliferation data at of A375 cells 96 h after different irradiation times as a function of the neutron fluence. Data corresponding to similar doses are grouped like in the left graphs. Values are expressed as absorbance given by the plate reader, normalized to control (non irradiated cells). Raw and processed data are available via [23]. Errors in dose correspond to standard deviation (SD) due to differences on irradiation times. Errors in survival and absorbance correspond to the highest error in between SD and the error propagation.

With these assumptions, the total survival fraction S is assumed to be the product of the two components S_γ (photon survival) and S_n (pure neutron survival):

$$S = S_\gamma \cdot S_n = e^{-\alpha_\gamma D_\gamma - \beta_\gamma D_\gamma^2} \cdot e^{-\alpha_n D_n} \quad (2)$$

For removing the photon effect of the beam, we have evaluated for each sample the pure neutron survival S_n from the experimental values of S and making use of Eq, (2) with the following data for the radiobiological photon parameters for A375 cells from Gómez-Millan et al. [24]: $\alpha_\gamma = 0.187 \pm 0.057\,\mathrm{Gy}^{-1}$ and $\beta_\gamma = 0.035 \pm 0.008\,\mathrm{Gy}^{-2}$.

The resulting $S_n$values are displayed in Fig. 8. A fitting of an exponential function to these values has been done with the result of $\alpha_n = 0.93 \pm 0.03\,\mathrm{Gy}^{-1}$. The fit is also illustrated in Fig. 8 (dotted line).

The fit was computed using the Levenberg-Marquardt algorithm [25]. The correlation coefficient was r = 0.998 and the reduced chi squared gives 0.124. The good agreement of the values of S_n in log scale with a linear function, characteristic of high LET radiation, shows the adequacy of the removal of the photon effect.

In Table 3 we show the dose contributions received by the different samples and the partial survival fractions.

In Fig. 9 we illustrate a comparison of the survival function in terms of the total absorbed dose for the pure neutron irradiation obtained in this work with the photon survival from the measurements of Gómez-Millán et al. [24] and with the survival data obtained in the mixed field beam. At a 1 Gy photon irradiation, the survival is around 80%, while 1 Gy of pure thermal neutron dose leads to a survival of less than 40%. The data obtained at the ILL is in between these two cases, because the dose is a mix of a contribution of thermal neutrons and a small

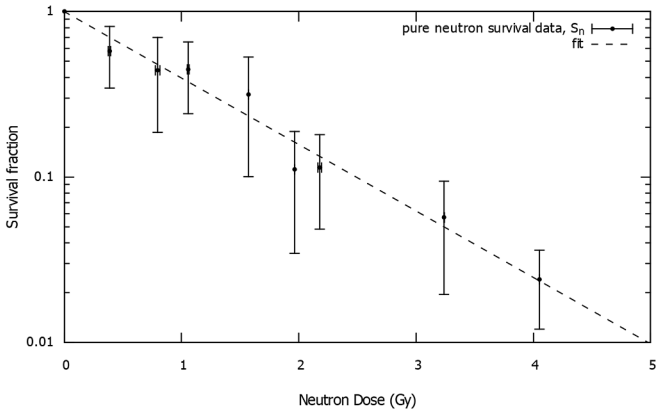

Fig. 8. Pure neutron survival fraction S_n data, extracted from the experimental survival as mentioned in the text, displayed in logarithmic scale in terms of the thermal neutron dose. The linear fit displayed with the dashed line gives a radiobiological coefficient of $\alpha_n = 0.93 \pm 0.03\,\mathrm{Gy}^{-1}$ for thermal neutrons.

percentage of photons. For a certain survival fraction, by the comparison of the dose of the curve following S_{ref} and the curve following S_n, the RBE can be obtained.

For obtaining the RBE factor w_t it is necessary to compare the photon and pure thermal neutron dose producing the same survival. This is intrinsically dependent on the survival (i.e. on the dose itself) and it is usually reported for different levels of survival. For a given D_n, the RBE factor is given by $w_t = D_{\gamma,ref}/D_n$, where $D_{\gamma,ref}$ denotes the reference photon dose producing the same survival, that can be calculated

Table 3
Values for each absorbed dose component of the irradiation (for each cuvette position and irradiation time): D_n for thermal neutrons, D_γ for the photons and D for the total. S is the final survival fraction of the A375 samples. Survival correponding to photon irradiation, S_γ, described with Gómez-Millan et al. (2012) parameters [24]. Values for the survival fraction corresponding to the effect of just the thermal neutron component of the beam, S_n, calculated using Eq. (2). Errors of *D* and *S* from measurements, as explained in Fig. 7 caption. Errors for all the other components by error propagation.

Sample	D(Gy)	D_γ(Gy)	D_n(Gy)	S	S_γ	S_n
Control	0.000 ± 0.000	0.000 ± 0.000	0.000 ± 0.000	1.000 ± 0.000	1.000 ± 0.000	1.000 ± 0.000
Cuvette 2, 15 min	0.552 ± 0.013	0.165 ± 0.004	0.386 ± 0.009	0.559 ± 0.220	0.969 ± 0.010	0.577 ± 0.233
Cuvette 1, 15 min	1.008 ± 0.023	0.212 ± 0.005	0.796 ± 0.018	0.423 ± 0.239	0.960 ± 0.013	0.441 ± 0.255
Cuvette 2, 40 min	1.510 ± 0.010	0.452 ± 0.003	1.057 ± 0.007	0.408 ± 0.148	0.912 ± 0.026	0.447 ± 0.206
Cuvette 2, 60 min	2.243 ± 0.001	0.672 ± 0.000	1.571 ± 0.001	0.274 ± 0.175	0.868 ± 0.036	0.315 ± 0.215
Cuvette 2, 75 min	2.759 ± 0.019	0.580 ± 0.004	2.179 ± 0.015	0.101 ± 0.005	0.887 ± 0.033	0.114 ± 0.066
Cuvette 1, 40 min	2.807 ± 0.001	0.841 ± 0.000	1.966 ± 0.001	0.093 ± 0.002	0.834 ± 0.045	0.111 ± 0.077
Cuvette 1, 60 min	4.100 ± 0.002	0.862 ± 0.000	3.239 ± 0.002	0.047 ± 0.028	0.829 ± 0.046	0.057 ± 0.037
Cuvette 1, 75 min	5.131 ± 0.002	1.079 ± 0.000	4.052 ± 0.001	0.019 ± 0.004	0.785 ± 0.056	0.024 ± 0.012

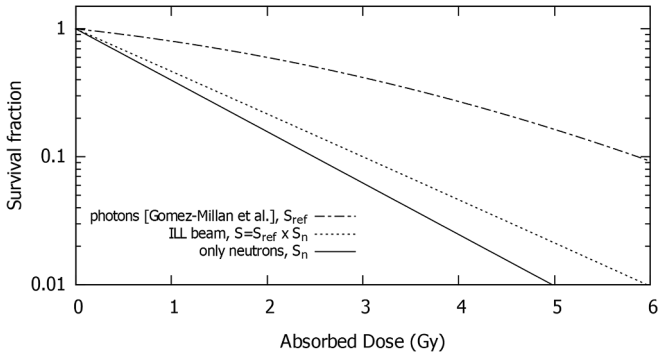

Fig. 9. Survival data from the A375 cells irradiated at ILL fitted with the survival function S. S_{ref} and S_n correspond to survival curves due to the isolated effect of photon and thermal neutron irradiation respectively, both described with the parameters included in the text (α_γ and β_γ for photons and α_n for neutrons).

(once knowing α_γ, β_γ and α_n) from

$$S_{RBE} = e^{-\alpha_\gamma D_{\gamma,ref} - \beta_\gamma D_{\gamma,ref}^2} = e^{-\alpha_n D_n} \quad (3)$$

By using the radiobiological coefficients of above, we find the results displayed in Table 4 for different common survival choices. Zero-dose limiting value, also called RBE_{max} or W_t, is included, which corresponds to the ratio between alpha coefficients: $W_t = \alpha_n/\alpha_\gamma$. For a particular application, the RBE value chosen should correspond to the actual thermal neutron dose D_n according to the treatment plan.

In reported BNCT treatments for melanoma [26], the mean thermal neutron dose is about 2.3 Gy (range of 1.3–3.5 Gy). From the observation of the table, this corresponds to values of the RBE in an interval of 2.4–2.8, close to the values used for the thermal dose both at skin and tumor in the melanoma clinical trials: 2.5 for the Kyoto trials [26] or 3.0 for the Argentinian ones [27], and smaller than the value of 3.2 used in brain tumor clinical trials [6].

Table 4
RBE values obtained for different survival fractions by the ratio of the reference photon dose and the neutron dose. Errors performed by error propagation.

Survival (%)	D_n(Gy)	Error D_n	$D_{\gamma,ref}$(Gy)	Error $D_{\gamma,ref}$	w_t(RBE)	Error w_t
100 – limit	Limit → 0		Limit → 0		**4.95 (W_t)**	1.81
75	0.311	0.011	1.247	0.029	4.01	0.39
50	0.749	0.025	2.519	0.027	3.36	0.67
37	1.075	0.037	3.290	0.025	3.06	0.68
25	1.498	0.051	4.166	0.024	2.78	0.65
10	2.488	0.085	5.868	0.023	2.36	0.58
5	3.238	0.110	6.958	0.022	2.15	0.54
1	4.977	0.169	9.106	0.021	1.83	0.47

In these data, the uncertainty from the fitting is less than 6%. However, the resulting uncertainties for the RBE values are of the order of 30%, due to the 30% uncertainty of the photon α coefficient taken from the literature. Therefore this procedure allows the collection of accurate data for low-energy neutrons so that more precise RBE factors can be calculated, provided photon data of similar precision become available.

4. Conclusions and outlook

The PF1b line at the ILL reactor provides a high flux of cold neutrons, with a low gamma component and the absence of an epithermal dose due to the bent neutron guide. This results in an ideal beam for measuring the radiobiological effect of thermal neutrons. In addition, with the new installation of a level 2 biological laboratory inside the neutron guide hall, it is possible to handle mammalian cells and carry out multiple irradiations and measurements per day, contributing to better statistics.

New data for the damage of thermal neutrons in melanoma cells have been obtained following the explained procedure. The RBE of thermal neutrons for this cell type can be calculated for different doses from Fig. 9. For BNCT melanoma treatments, a RBE factor from Table 4 can be chosen according to the thermal dose applied.

The developed setup at PF1B-ILL paves the way to extensive measurements, following the same procedure for other cell lines of both, tumor and healthy cells. An experimental campaign has been started at ILL for this purpose. This can be of interest not only for BNCT but also for the extraction of data for radioprotection purposes. As the boron dose in BNCT is produced by thermal neutrons, in this campaign the measurement of the boron RBE factor (compound-dependent CBE) for different compounds is also foreseen, using the same setup and procedure described here.

Declaration of Competing Interest

The authors declare that they have no known competing financial interests or personal relationships that could have appeared to influence the work reported in this paper.

Acknowledgments

We acknowledge financial support for this work from the Fundación Científica de la Asociación Española Contra el Cáncer (AECC) under grant PS16163811PORR, Junta de Andalucía (Andalusian Regional Government), under contract P11-FQM-8229, Spanish MINECO and FEDER funds under contract FIS2015-69941-C2-1-P, the grant agreement ILL-UGR and the founders of the University of Granada Chair Neutrons for Medicine: Spanish Fundación ACS and Capitán Antonio. M.P. acknowledges a grant under the program Becas de Iniciación a la

Investigación from the Universidad de Granada (Plan Propio de Investigación). The open access fee was covered by FILL2030, a European Union project within the European Commission's Horizon 2020 Research and Innovation programme under grant agreement N°731096.

Appendix A. Supplementary data

Supplementary data to this article can be found online at https://doi.ill.fr/10.5291/ILL-DATA.3-07-376.

References

[1] R.F. Barth, et al., Current status of boron neutron capture therapy of high grade gliomas and recurrent head and neck cancer, Radiat. Oncol. 7 (2012) 146.
[2] A.J. Kreiner, et al., Present status of accelerator-based BNCT, Rep. Pract. Oncol. Radiother. 21 (2016) 95.
[3] IAEA 2001 Current status of neutron capture therapy IAEA-TECDOC-1223 ISSN 1011–4289.
[4] J.T. Goorley, W.S. Kiger III, R.G. Zamenhof, Reference dosimetry calculations for neutron capture therapy with comparison of analytical and voxel models, Med. Phys. 29 (2002) 145.
[5] J.A. Coderre, G.M. Morris, The radiation biology of boron neutron capture therapy, Radiat. Res. 151 (1999) 1.
[6] J.A. Coderre, et al., Derivations of relative biological effectiveness for the high-LET radiations produced during boron neutron capture irradiations of the 9L rat glio-sarcoma in vitro and in vivo, Int. J. Radiat. Oncol. Biol. Phys. 27 (1993) 1121.
[7] E. Bavarnegin, Y. Kasesaz, F.M. Wagner, Neutron beams implemented at nuclear research reactors for BNCT, J. Instrum. 12 (2017) 05005.
[8] J.W. Hopewell, G. Morris, A. Schwint, J.A. Coderre, The radiobiological principles of boron neutron capture therapy: a critical review, Appl. Radiat. Isot. 69 (2011) 1756.
[9] E.J. Hall, et al., RBE as a function of neutron energy: I Experimental observations, Radiat. Res. 64 (1975) 245.
[10] G.R. Morgan, et al., The radiobiology of 24 keV neutrons, Br. J. Radiol. 61 (1988) 1127.
[11] J.-P. Hu, N.E. Holden, R.N. Reciniello, Dosimetry in Thermal Neutron Irradiation Facility at BMRR. EPJ Web of Conferences, EDP Sci. 106 (2016).
[12] S. Bortolussi, et al., Neutron flux and gamma dose measurement in the BNCT irradiation facility at the TRIGA reactor of the University of Pavia, Nucl. Instrum. Methods Phys. Res., Sect. B 414 (2018) 113.
[13] I. Auterinen, et al., Measurement of free beam neutron spectra at eight BNCT facilities worldwide, Appl. Radiat. Isot. 61 (2004) 1021.
[14] H. Abele, et al., Characterization of a ballistic supermirror neutron guide, Nucl. Instrum. Methods Phys. Res., Sect. A 562 (2006) 407.
[15] M. Jentschel, et al., EXILL—a high-efficiency, high-resolution setup for γ-spectroscopy at an intense cold neutron beam facility, J. Instrum. 12 (2017) 11003.
[16] D.B. Pelowitz, MCNPX Users Manual Version 2.5.0 - LA-CP05-0369, Los Alamos National Laboratory, 2005.
[17] K. Lefmann, K. Nielsen, McStas, a general software package for neutron ray-tracing simulations, Neutron News 10 (1999) 20.
[18] S.M. Seltzer, Calculation of photon mass energy-transfer and mass energy-absorption coefficients, Radiat. Res. 136 (1993) 147.
[19] M.A. Lone, D.C. Santry, W.M. Inglis, MeV neutron production from thermal neutron capture in Li and B compounds, Nucl. Instrum. Methods 174 (1980) 521.
[20] S. Frankel, A.J. Reiches, A.J.V. O'Toole, Nitrogenous composition of human epidermis: I. free amino acids, total nitrogen, non-protein nitrogen, urea, and ammonia in post-surgical and post-mortem epidermis, J, Invest. Dermatol. 36 (1961) 83.
[21] G. Allavena, et al., Trehalose inhibits cell proliferation and amplifies long-term temozolomide-and radiation-induced cytotoxicity in melanoma cells: a role for autophagy and premature senescence, J. Cell. Physiol. 234 (2019) 11708.
[22] J.F. Fowler, The linear-quadratic formula and progress in fractionated radiotherapy, Br. J. Radiol. 62 (1989) 679.
[23] I. Porras et al., Radiobiology in vitro measurements for Boron Neutron Capture Therapy, Institut Laue-Langevin (2018). https://doi.ill.fr/10.5291/ILL-DATA.3-07-376.
[24] J. Gómez-Millán, et al., The importance of bystander effects in radiation therapy in melanoma skin-cancer cells and umbilical-cord stromal stem cells, Radiother. Oncol. 102 (2012) 450.
[25] W.H. Press, S.A. Teukolsky, W.T. Vetterling, B.P. Flannery, Numerical Recipes: The Art of Scientific Computing, Cambridge University Press, Cambridge, 2007.
[26] H. Fukuda, et al., Boron neutron capture therapy (BNCT) for malignant melanoma with special reference to absorbed doses to the normal skin and tumor, Australas. Phys. Eng. Sci. Med. 26 (2003) 97.
[27] H.R. Blaumann, et al., Boron neutron capture therapy of skin melanomas at the RA-6 reactor: a procedural approach to beam set up and performance evaluation for upcoming clinical trials, Med. Phys. 31 (2004) 70.